Auton Robot
DOI 10.1007/s10514-013-9336-1

# Optimal spatial formation of swarm robotic gas sensors in odor plume finding

**Ali Marjovi · Lino Marques**

Received: 10 August 2012 / Accepted: 2 May 2013


**Abstract** Finding the best spatial formation of stationary gas sensors in detection of odor clues is the first step of searching for olfactory targets in a given space using a swarm of robots. Considering no movement for a network of gas sensors, this paper formulates the problem of odor plume detection and analytically finds the optimal spatial configuration of the sensors for plume detection, given a set of assumptions. This solution was analyzed and verified by simulations and finally experimentally validated in a reduced scale realistic environment using a set of Roomba-based mobile robots.

**Keywords** Odor plume finding · Olfactory search · Swarm robotics formation · Gas sensor coverage

## 1 Introduction

Searching for olfactory targets with mobile robots has received much attention in the recent years. This problem finds applications in environmental monitoring (Dunbabin and Marques 2012), chemical leak detection (Russell et al. 1995), pollution monitoring (Fu et al. 2012), inspection of landfills (Hernandez Bennetts et al. 2012), and search and rescue operations (Wang et al. 2010). Some of these tasks are done in scenarios extremely dangerous for humans, being desirable to use robots instead.

The effort to design and develop robotic olfactory search strategies faces the problem of understanding how the odor molecules disperse in the environments under naturally turbulent flow. Odor patches released by an odor source are mainly transported by the airflow, forming an odor plume. As the plume travels away from the source, it becomes more diluted due to molecular diffusion and turbulence that mixes the odor molecules with the clean air (Roberts and Webster 2002). Molecular diffusion is a slow process whose effect on the plume shape can be neglected. The dispersion of odor molecules is dominated by flow turbulences in ventilated indoor or in outdoor environments. The odor molecules move downwind due to mean flow velocity **U** while their net motion is a random walk due to the fluctuations. In large scale environments, fluctuations happen also in the initial direction of the plume that create undulating and meandering patterns. The flow carries patches of odor while the amplitude of the concentration within a patch decreases away from the source, and the average time between two successive patches increases. At high Reynolds numbers, the instantaneous odor concentration strongly fluctuates intermittently with peaks above three orders of magnitude around the average concentration value (Crimaldi et al. 2002). Under these circumstances, a chemical sensor located far enough downwind of the odor source, most of the time measures no odor concentration. The probability of encountering an odor patch at any given point is determined by the relative location in between the odor source and the sensor, the statistics of the flow and the shape of the environment and the obstacles (Sutton 1947; Gifford 1960). The velocity of the airflow is set by the environmental conditions and hence stays unchanged for long periods of time compared with the time scale of odor fluctuations. Figure 1 presents the nature of an odor plume from different scales.

Finding the odor plume in environments with high Reynolds numbers, i.e., searching the environment randomly or systematically in order to find odor clues, is the final goal

A. Marjovi (✉) · L. Marques
Institute of Systems and Robotics, University of Coimbra, 3030-290 Coimbra, Portugal
e-mail: marjovi@gmail.com; ali@isr.uc.pt

L. Marques
e-mail: lino@isr.uc.pt

Published online: 17 May 2013

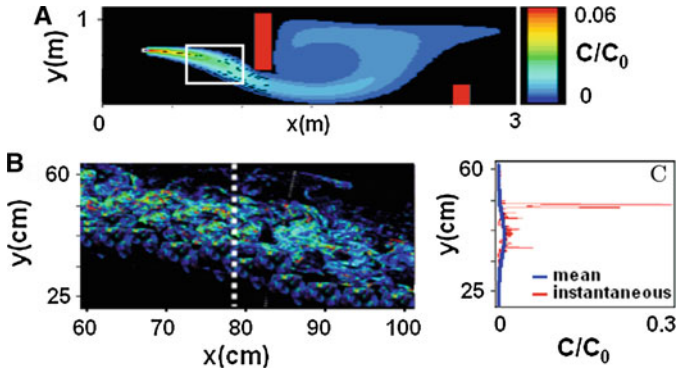


**Fig. 1** Distribution of odor patches in an environment with obstacles when the wind direction is from *left* to *right*. **a** Mean structure of odor distribution (measured by slow-response gas sensors), **b** instantaneous structure of a part of the odor plume (measured by fast-response gas sensors), and **c** an instantaneous and a mean cross-wind slice of (**a**) and (**b**) (measured by moving a fast and a slow gas sensor towards cross-wind). Image is adapted from Crimaldi et al. (2002)

of this study. This is the first phase in search for odor sources (Hayes et al. 2003). The second phase is plume tracking, that is, following the plume toward the source, and final step is source declaration, that is, accurately localizing the source in close vicinity. Most of the works concerning olfactory search have focused on odor plume tracking (Martinez et al. 2006; Li et al. 2001; Lochmatter and Martinoli 2009; Lytridis et al. 2006) whereas plume finding has received little attention. Concentration gradient climbing [chemotaxis (Russell et al. 2003; Grasso et al. 1997)] and up-wind directed search [anemotaxis (Marques and de Almeida 2006; Marjovi and Marques 2011; Lochmatter et al. 2010)] are the most common approaches to track odor plumes by mobile robots. Several other methods have been proposed for plume tracking using swarm robotic concepts, namely, biasing expansion swarm approach (Cui et al. 2004), biased random walk (BRW) (Marques et al. 2002), particle swarm optimization (Li et al. 2008; Marques et al. 2006), glowworm swarm optimization (Krishnanand and Ghose 2008), gradient climbing techniques (Marjovi et al. 2010b), swarm spiral surge (Kazadi 2003), and physics-based swarming approach (Zarzhitsky et al. 2005). Most of these studies (e.g. Grasso et al. 1997; Kowadlo et al. 2006; Vergassola et al. 2007) assume that the robots start their search within or very near the plume. Plume finding problem is usually addressed through general exploration methods (Marjovi et al. 2009, 2010a; Marjovi and Marques 2012), mapping (Loutfi et al. 2008; Lilienthal and Duckett 2004), or coverage techniques namely zig-zag sweeping, casting (Pyk et al. 2006), random wandering (Ishida et al. 2006), BRWs (Marques et al. 2002), lévy-taxis (Pasternak et al. 2009), and spiral movements (Ferri et al. 2009), which are also used for other spatial search tasks and are not specifically designed for odor plume finding.

A mobile sensor network can be advantageous in odor plume finding tasks, in comparison to a single robot that can measure only the odor concentration on its own place. The airflow that carries the odor patches can be very irregular and chaotic, thus the resulting distribution of odor concentration may be also very irregular with large intermittency in the region downwind an odor source. Additionally, the search space may be much larger than the active area of an odor source. In these conditions, using multiple sensing nodes spread throughout the environment improves the detection process, increasing the probability of finding an odor plume in a given time. A swarm of robots can establish a dynamic mobile sensor network and move in the area of interest to find the plume. To efficiently address the problem of odor plume finding by a swarm of robots, one should answer the following questions:

1. What is the best spatial formation for the swarm robots in searching for an odor plume?
2. What is the best movement strategy for the swarm in odor plume searching?

None of the works neither in the olfactory search area nor in the swarm robotics field has ever answered these questions. This paper addresses the first challenge using a novel swarm approach in an environment under turbulent airflow.

To state the problem, consider a swarm of $N$ robots that are able to communicate with each other over a distance $\Delta_d$ and are equipped with olfactory sensors for sensing the odor concentration $\bar{C}$ and airflow speed $\mathbf{U}$. There is no central controller for the system, so the robots act independently. The problem is: "what is the best spatial formation strategy for the swarm in search for an odor plume in an area?".

Recently, a few studies were reported that tackle the problem of optimal gas sensor deployment mainly for safety systems in process facilities. Legg et al. (2012) presented a method that utilizes computational fluid dynamics (CFD) simulations to optimize gas sensor locations in order to maximize the likelihood of early detection of gas clouds in specific facilities. Miyata and Mori (2011) introduced another procedure for optimization of gas detector locations by using gas

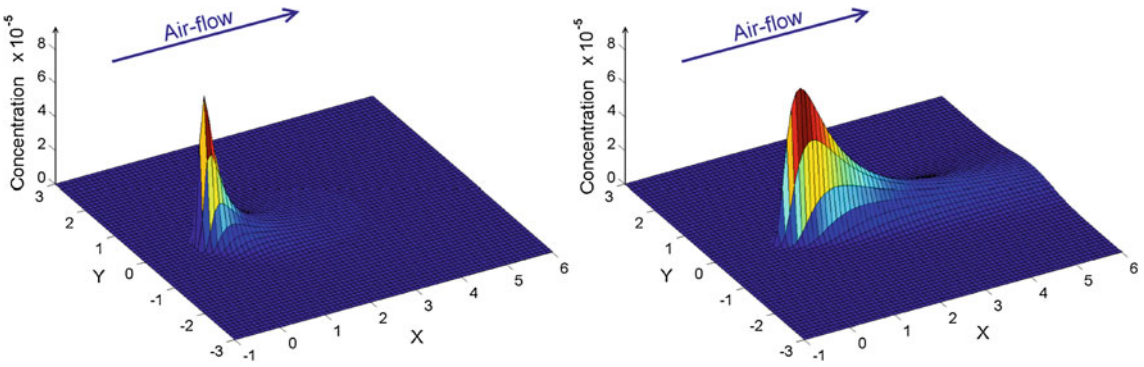


**Fig. 2** The mean concentration in the 2D plane of $z = 0.1$ m. source location:(0, 0, 0), release rate = 0.01 g/s and $\bar{U} = 1$ m/s. *Left* A–B conditions, *right* E–F conditions

dispersion simulation tools in specific chemical plants. However, in these studies, the gas source location (leak point) and the map of environment were both a-priory known, and simulations were run to find the best sensors' positions among a list of candidate locations. A-priory knowing the source location and the map of the environment and having a list of candidate positions for the sensors are three assumptions that we do not make in this paper. Moreover, instead of CFD simulations, this paper provides analytical results using gas dispersion models.

This paper presents an analytical method to find the optimal spatial formation of swarm robots in plume finding strategies (described in Sect. 2). Defining single and multiple gas sensors coverage and finding the optimal configuration of N mobile sensors in different environmental conditions are among the main novelties of this paper. Moreover, based on the results of optimizations, we present and design a set of wind-biased virtual attractive/repulsive control forces for the swarm robots such that their emergent behavior converges to the optimal formations (explained in Sect. 3). None of the previously designed control systems in olfactory robotics community has ever biased the virtual forces by the wind effect. The proposed method was validated and evaluated by simulation and experimented in small scale realistic environments (in Sect. 4).

## 2 Optimal coverage with gas-sensors

This section finds the best configuration of robots to maximize their sensing coverage area and then Sect. 3 designs swarming behaviors of individual robots to reach to the found configurations.

### 2.1 Odor dispersion model

Probability density function of odor dispersion in a turbulent medium is represented by the Gaussian model for odor distribution in average-term exposure (Sutton 1947; Gifford 1960; Roberts and Webster 2002). The Gaussian plume models yield results that match experimental results reasonably well (Jones 1983). If an odor source is located in position (0, 0, 0), its release rate is $Q$ and the average wind speed is $\bar{U}$ toward x-axis (Fig. 2), then, the mean concentration of odor in position (x, y, z) is given by the following probability density function:

$$\bar{C}(x, y, z) = \frac{Q}{2\pi \bar{U} \sigma_y(x) \sigma_z(x)} \exp\left\{ \frac{-y^2}{2\sigma_y^2(x)} + \frac{-z^2}{2\sigma_z^2(x)} \right\} \quad (1)$$

where x, y, and z (here and throughout this article) denote the downwind, crosswind, and vertical position coordinates relative to the odor source with x positive along the mean wind direction $\overrightarrow{U}$.

The standard deviations $\sigma_y(x)$ and $\sigma_z(x)$ model the horizontal and vertical dispersion of the plume. These standard deviations are not constant. It was found experimentally by Briggs (1973) that both parameters are functions of the downwind distance from the source $(x)$ according to the environmental conditions, as expressed in Table 1. In this table the following environmental conditions are considered; A: neutral, B: slightly stable, C: stable, D: isothermal, E: moderate inversion, F: strong inversion.

Figure 2 demonstrates the mean concentration in a 2-D plane of $z = 0.1$ m, generated from an odor source at (0, 0, 0)

**Table 1** Standard deviations for an urban environment in various environmental conditions (Briggs 1973)

| Env. | $\sigma_y(x)$ | $\sigma_z(x)$ |
|---|---|---|
| A–B | $0.32x(1+0.0004x)^{-0.5}$ | $0.24x(1+0.001x)^{0.5}$ |
| C | $0.22x(1+0.0004x)^{-0.5}$ | $0.20x$ |
| D | $0.16x(1+0.0004x)^{-0.5}$ | $0.14x(1+0.0003x)^{-0.5}$ |
| E–F | $0.11x(1+0.0004x)^{-0.5}$ | $0.08x(1+0.0015x)^{-0.5}$ |

when release rate is 0.01 g/s and wind speed is 1 m/s toward the x-axis direction, in neutral/slightly stable (A–B) (left) and moderate/strong inversion (E–F) (right) environmental conditions, based on Eq. (1) and Table 1.

### 2.2 Gas sensor area coverage

Most gas sensors show pseudo-linear responses to gas concentrations (Arshak et al. 2004). Considering the odor dispersion model in (1) at a fixed height (z = constant = source height) this 3D phenomena can be treated as a 2D problem. Similar to Balkovsky and Shraiman (2002) and Meng et al. (2011), we conclude that if an odor source is at $O(x_0, y_0)$, the conditional probability of detecting odor patches by a stationary gas sensor located in position $(x, y)$ is given by:

$$P\left(D_{xy}|O_{x_0y_0}\right) = \frac{kQ}{2\pi\bar{U}\sigma_y(x)\sigma_z(x)} \exp\left\{-\frac{(y-y_0)^2}{2\sigma_y^2(x)}\right\} \quad (2)$$

where $k$ is the sensitivity parameter of a gas sensor to the odor concentration. In other words, if a sensor is located in position $(x, y)$, its probability of detecting an odor patch released from a source located in position $(x_0, y_0)$ is given by $P\left(D_{xy}|O_{x_0y_0}\right)$ in (2). Equation (2) defines that the higher the concentration of the odor, the higher the probability of detecting by a sensor. It should be mentioned that the environment in this model (and throughout this paper) is presented by uniform grid maps, so any Cartesian (x, y) denotes a grid cell with center at (x, y). Another point is that since this equation presents a probability function, its result is truncated to [0, 1]. Although this equation has been simplified by considering $z = constant = z_0$, standard deviations of vertical direction ($\sigma_z(x)$) exists and plays a significant role in this probability function. From 2, if there is a gas sensor at a given position $(x, y)$, where $(y-y_0) \gg \sigma_y(x)$, its probability of finding an odor patch is very small. Figure 3 is an example that presents the distribution of this probability when a sensor is located at (0, 0), $\bar{U}$ is 1 m/s, and the environmental is in moderate/strong inversion conditions (E–F type). As it is shown in Figs. 2 and 3, the odor plume emitted from a source shapes toward the airflow direction, whereas, the probability of detection of a gas sensor shapes in the opposite direction of the airflow.

Given N independent sensors $s_i$ located at $(x_i, y_i)$, $i = 1 \ldots N$, we compute the total probability $P\left(D_N\middle|O(x_j, y_j)\right)$, due to the combined efforts of all sensors, of detecting odor patches released from a source in $O(x_j, y_j)$. This probability is one minus the probability that all sensors fail to detect:

$$P\left(D_N\middle|O(x_j, y_j)\right) = 1 - \prod_{i=1}^{N}\left\{1 - P\left(D_{x_iy_i}|O_{x_jy_j}\right)\right\} \quad (3)$$

In other words, if an odor source is located at $O(x_j, y_j)$, the probability that at least one sensor (from N applied sensors) detects odor patches is given by $P\left(D_N\middle|O(x_j, y_j)\right)$ in (3).

The probability functions (2) and (3) inherently define a probabilistic coverage area for the sensors. To obtain the area covered by the gas sensors, a sensitivity threshold $S_{th}$ for the probability of odor patch detection should be considered. This is based on the fact that most of the gas sensors show a sensitivity threshold i.e. bellow a certain value of odor concentration, the sensors do not detect any odor patch. Thus, this paper defines the binary coverage area of a gas sensor as following:

**Definition 1** (*single gas sensor binary coverage*) Given a sensor $s_i$ in position $(x_i, y_i)$ and a point of interest $p_j = (x_j, y_j)$ the coverage of the sensor $s_i$ to the point $p_j$ is defined as:

$$cover(s_i, p_j) = \begin{cases} 1, & P\left(D_{x_iy_i}|O_{x_jy_j}\right) > S_{th} \\ 0, & Otherwise \end{cases} \quad (4)$$

where $P\left(D_{x_iy_i}|O_{x_jy_j}\right)$ is given by (2). Figure 4a presents the coverage area of one gas sensor when the wind is toward up direction. Despite most of the coverage areas of different types of sensors (e.g. acoustic, thermal, vision) which are either circular or directional sectors towards sensor's head-

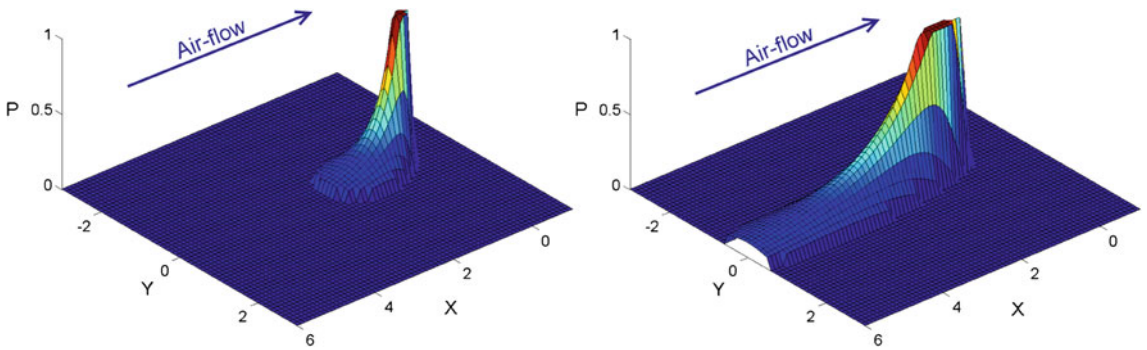


**Fig. 3** The probability of detecting odor patches by a sensor at (0, 0) if the odor source is located in various points in the plane $z = z_0 = 0$, when k = $10^5$, source release rate = 0.01 g/s and $\bar{U}$ = 0.5 m/s in in A–B environmental conditions (*left*), and E–F environmental conditions (*right*) (Table 1)

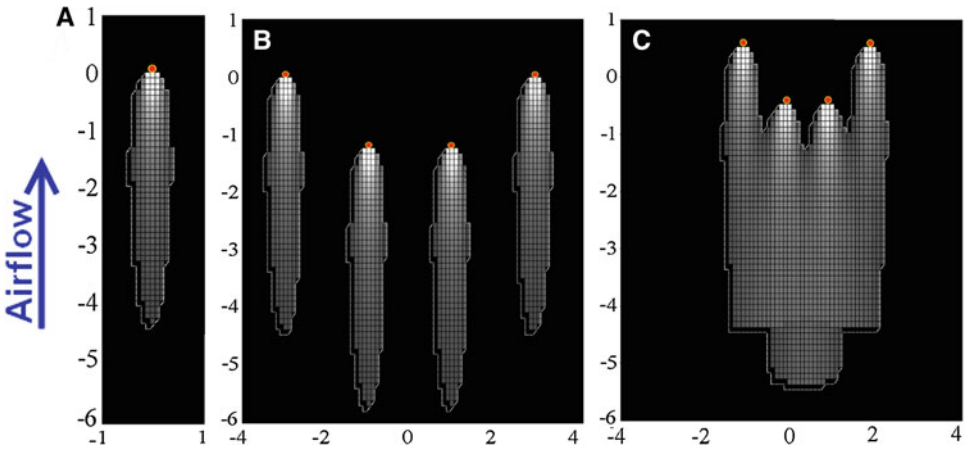


**Fig. 4** Arbitrary placement of sensors and their coverage area when $S_{th} = 0.3$, $k$=$10^5$, $Q$=0.01 g/s, and $U$=0.2 m/s in strong inversion conditions. The *red circles* show the gas sensors and the *white regions* represent the probabilistic coverage area. *Note* the coverage area in (**c**) is larger than in (**b**) (Color figure online)

ing, the coverage are of gas sensors is ellipsoid shape biased towards the wind direction.

With the knowledge of the coverage between sensor $s_i$ and all points of interest, the overall coverage by sensor $s_i$ can be defined by aggregation. If there are $m$ points of interest, then the total coverage by a sensor $s_i$ is defined as:

**Definition 2** (*overall coverage by a sensor*) The overall coverage "$cover(s_i)$" by a sensor $s_i$ over a region with $m$ points of interest in $R^2$ is given by:

$$cover(s_i) = \sum_{j=1}^{m} cover(s_i, p_j) \tag{5}$$

In this paper, $m$ is the total number of grid cells of a region.

Given N sensors $s_i$ located at $(x_i, y_i)$, $i = 1 \ldots N$, we define their combined coverage to the point $p_j$ as:

**Definition 3** (*N gas sensors binary coverage*) The combined binary coverage of N sensors $s_i, i = 1 \ldots N$ on a point $p_j$ is defined as:

$$cover(S, p_j) = \begin{cases} 1, & P\left(D_N \middle| O(x_j, y_j)\right) > S_{th} \\ 0, & Otherwise \end{cases} \tag{6}$$

$P\left(D_N \middle| O(x_j, y_j)\right)$ is given by Eq. (3) and is the combined probability of detection of odor patches if the odor source is located at $(x_j, y_j)$ by N sensors and $S$ denotes the set of $(x_i, y_i)$ positions of the sensors. Although the coverage is defined in binary form, its nature is still probabilistic.

Finally, the overall coverage of N sensors over a region is defined by:

**Definition 4** (*overall coverage by N sensors*) The overall coverage "$cover(S)$" by N sensors $s_i$, $i = 1 \ldots N$ over a region with $m$ points of interest in $R^2$ is given by:

$$cover(S) = \sum_{j=1}^{m} cover(S, p_j) \tag{7}$$

This equation implies that the overall coverage is a function of sensors' positions, source release rate, average wind speed, sensors sensitivity, and distribution standard deviations related to environmental conditions.

Using these equations, Fig. 4b and c present the coverage area of four sensors in two different configurations. It should be pointed out that, the coverage area in Fig. 4c is larger than the coverage area in Fig. 4b, meaning that the coverage area of N sensors depends on their spatial topology.

### 2.3 Optimal sensor deployment

Optimal sensor deployment aims to position the sensors in a way that overall coverage is maximized. Thus, we are looking for a series of sensors positions $s_i = (x_i, y_i)$ such that:

$$\{s_1, s_2, \ldots s_N\} = \arg\max cover(S)$$

Optimal sensor positions are where the coverage area of the sensors is maximized. Therefore maximizing the area of sensor coverage, defined in (7), is used as the criterion of our optimization. We optimize this criterion with various number of sensors and different average wind speeds in four environmental conditions. Without loss of generality, we assume constant values for the following parameters during the optimizations: $S_{th} = 0.35$, $Q = 0.01$ g/s, $k = 10^5$ and the environment size is $50 \times 50$ m. These values are close to real world experimental measurements (Cheng et al. 2011).

The Powell's conjugate gradient descent method (Press et al. 2002) was used (in Matlab) to optimize this problem, since it does not need the derivative of the function and its convergence is fast even in high dimensional spaces. N sensors on a 2-D plane require 2N dimensional search space. For each combination of sensors' position, the coverage area is computed. The solution is a set of positions for sensors that its coverage area is the largest.

### 2.4 Optimization results

Figure 5 shows examples of optimized positions of two, four and eight sensors and their maximum coverage area in an

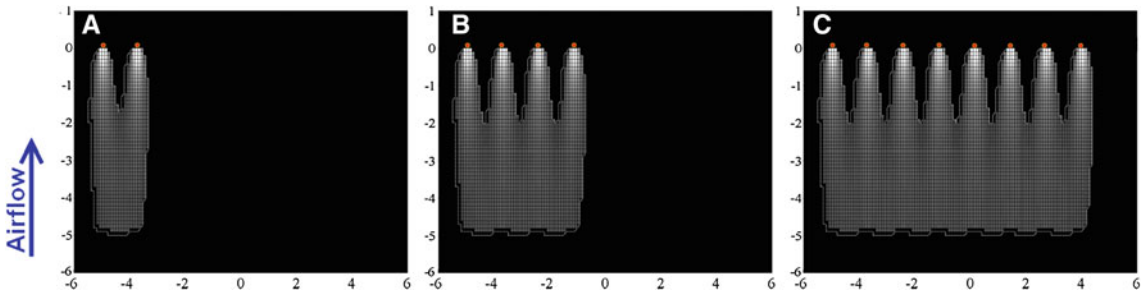


**Fig. 5** The optimized configuration of two, four and eight gas sensors in an area when the wind-speed is 0.2 m/s [moderate/strong inversion (E–F) conditions]. The *coverage area* in (**b**) is larger than in Fig. 4b and also Fig. 4c and any other configuration of 4 sensors

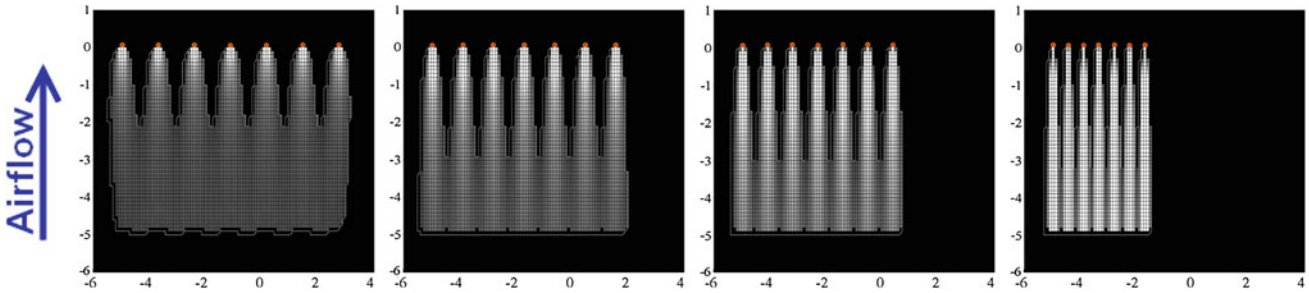


**Fig. 6** The optimized configuration of seven gas sensors in an area when the wind speed is 0.2, 0.5, 2, and 4 m/s (from *left* to *right* respectively) in moderate/strong inversion (E–F) environmental conditions

environment under moderate/strong inversion (E–F) conditions when the wind speed is equal to 0.2 m/s. Different values of $U$, and $N$ in different environmental conditions result in similar (but not equal) solutions. Figure 6 shows another example of optimized positions of seven sensors with different values for the wind speed. The optimal coverage area was measured for different number of sensors from 3 to 16, and different wind speeds from 0.1 to 15 m/s in the four environmental conditions listed in Table 1. The topological shape of the sensors in the optimal solutions was analyzed in each case.

One interesting point from all of the optimized solutions is that:

**Conclusion 1** (cross-wind line topology) *The topology of all of the optimal solutions is* ***line*** *configuration towards cross wind direction, with equal distance between each pair of neighboring sensors.*

Figure 7 is an example that shows the optimal distance between the neighboring sensors in the optimized configuration in neutral/slightly stable (A–B) and moderate/strong inversion (E–F) environmental conditions when the number of sensors is 3–16. Although this chart only shows the optimal results when the environmental conditions is A–B and F–E types (see Table 1, for the other environmental conditions, the obtained results for the same number of sensors were similar to this figure. By analyzing these results of the optimizations, it can be seen than, in constant wind speed, when the number of sensors changes (from 3 to 16), the optimal distance

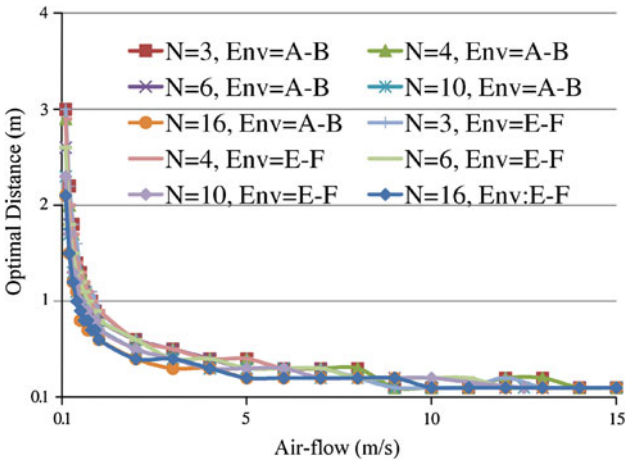


**Fig. 7** The optimal distance between the neighboring sensors in the optimized configurations. Number of sensors (N) varies from 3 to 16, environmental conditions (Env) is listed in Table 1, and the airflow is between 0.1 to 15 m/s

between the sensors changes only for a few centimeters and is almost constant even in various environmental conditions (see the examples in Figs. 5 and 7). Therefore:

**Conclusion 2** (wind dependent distance) *The distance between neighboring pairs in optimal configurations depends mainly on the wind speed, whereas, the number of sensors and the environmental conditions do not show significant impact on optimal configurations.*

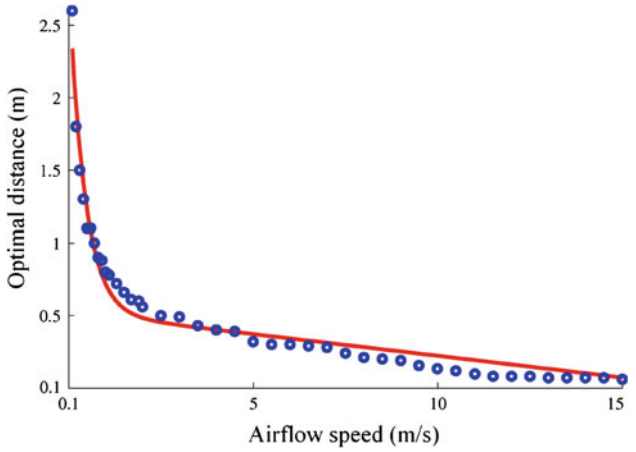


**Fig. 8** The average optimal distance between neighboring sensors in different airflow speeds in different environmental conditions (Color figure online)

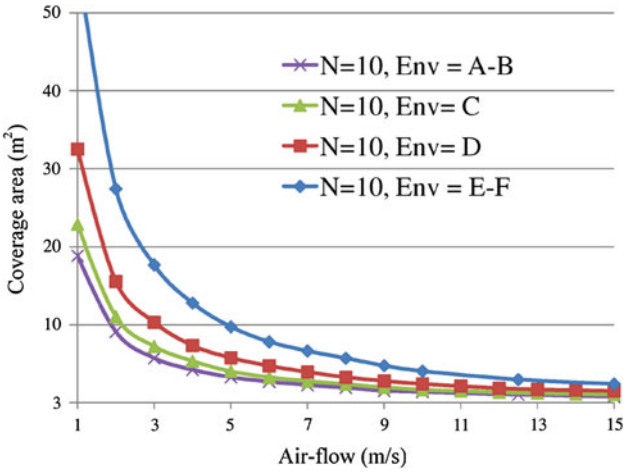


**Fig. 9** The maximum coverage area of 10 gas sensors in 4 different environmental conditions while the airflow varies from 0.1 to 15 m/s

These conclusions are drawn after the results obtained from numerical simulations and are the most significant contributions of this paper. The results in Fig. 7 show that **the higher wind speed, the smaller the optimal distance**. Therefore, as the wind speed increases, the distance in-between the sensing nodes should decrease in order to maintain optimal coverage however, when the wind speed decreases they should get apart and keep a larger distance in order to maximize their coverage area. Figure 8 shows the average optimal distance between neighboring sensors in different airflow speeds in different environmental conditions.

Taking the results shown in Fig. 8 and using a non-linear regression analysis, the following analytical equation was obtained that describes the optimal distance between the sensing nodes as a function of the wind speed in E–F (inversion) environmental conditions:

$$f(U) = 2.19e^{-2.81U} - 0.03U + 0.53 \tag{8}$$

Since the results of optimizations (in Fig. 7) is similar for various environmental conditions, we consider the average of optimal distances between neighboring sensors in different airflow speeds in all environmental conditions and obtain the following formula:

$$f(U) = 2.28e^{-2.3U} - 0.03U + 0.52 \tag{9}$$

The red line in Fig. 8 is the fitted function (9) and the scattered blue circles are the results of the optimizations. The mean square error of this regression line is $7.3 \times 10^{-3}$. This function is later used by moving senor robot to estimate the optimal distance based on the wind speed.

Figure 9 presents the overall coverage area achieved by 10 sensors in the optimal configurations in four different environmental conditions. Similar results were obtained considering other numbers of gas sensors. Although the optimal distance for the neighboring sensors is not dependent to the environmental conditions or to the number of sensors, Fig. 9 shows that when the environment is under moderate/strong inversion conditions, the coverage area of a group of gas sensors is larger than when the environmental conditions is neutral/slightly stable. On the other hand, in constant environmental conditions, **when the wind speed is lower the coverage area increases**. Therefore, in a windy environment more sensors are required to cover a given area.

It should be mentioned that the obtained results are valid for specific values of $S_{th}$, $k$ and $Q$ defined in Sect. 2.3, however, for other values the optimal configuration for the sensors is the same (i.e. a cross-wind line) and only the values of the optimal distance between the sensors and regression function (9) are changed. This process of optimization can be repeated and optimal results can be achieved in other conditions.

## 3 Wind-biased potential fields

From the optimization results, we conclude that, to maximize the probability of detecting odor plumes by a swarm, the robots should line-up cross-wind with equal distances from each other. There is no central node for swarm robots and the formation topology of the swarm is the emergent result of individual robots movements. Therefore, for the swarm to have a desired formation topology, each robot should move in the space with a correct and well-defined control manner. To control the motion of the robots to reach the optimal formations, this paper presents a novel method based on the virtual attraction/repulsion forces (Gazi and Passino 2004). Despite previous works on swarm formations, we take the wind direction and the wind speed into account and bias the attraction/repulsion forces by the wind to implement the desired cross-wind line-up formation. This method is a suit-

able control strategy for the swarming robots since it does not need a central control node and it is flexible to be modified to impediment other robotic behaviors (e.g obstacle avoidance). We define a behavior named "cross-wind line-up" for the individual robots in order to implement line formation for the swarm. This behavior defines two types of virtual forces that are applied to the robots; robot-to-robot and robot-to-environment forces.

### 3.1 Robot-to-robot forces

To line-up the robots toward the cross-wind direction, each robot measures the air-flow direction $\overrightarrow{U}$ and assumes this direction as its internal X-axis coordinate system and then it measures the relative distance to its neighboring robots. Then, the robots try to minimize their X-axis distances from their neighbors and maintain a constant distance with them in their Y-axis. Hence, we define a nonlinear bounded potential between each pair of neighboring robots $i$ and $j$ at time $t$:

$$< \overrightarrow{X}\ axis > \ \equiv \ < \overrightarrow{U} > \tag{10}$$

$$\overrightarrow{F}^{ij}_{cr}(t) = \overrightarrow{Fx}^{ij}_{cr}(t) + \overrightarrow{Fy}^{ij}_{cr}(t) \tag{11}$$

$$\overrightarrow{Fy}^{ij}_{cr}(t) = \begin{cases} -\mu_1\left(\frac{\|\overrightarrow{Y}_{ij}\|-D_1}{\|p_{ij}(t)\|^2}\right)\left[\frac{\overrightarrow{Y}_{ij}}{\|\overrightarrow{Y}_{ij}\|}\right], & 0 < \|\overrightarrow{Y}_{ij}(t)\| < D_1 \\ -\mu_2\left(\frac{\|\overrightarrow{Y}_{ij}\|-D_1}{\|p_{ij}(t)\|^2}\right)\left[\frac{\overrightarrow{Y}_{ij}}{\|\overrightarrow{Y}_{ij}\|}\right], & D_1 < \|\overrightarrow{Y}_{ij}(t)\| < D_2 \\ 0, & \|\overrightarrow{Y}_{ij}(t)\| > D_2 \end{cases} \tag{12}$$

$$\overrightarrow{Fx}^{ij}_{cr}(t) = \begin{cases} -\mu_3 \overrightarrow{X}_{ij}\left[\frac{1}{\|p_{ij}(t)\|^2}\right], & 0 < \|\overrightarrow{X}_{ij}(t)\| < D_2 \\ 0, & \|\overrightarrow{X}_{ij}(t)\| > D_2 \end{cases} \tag{13}$$

$$D_1 = 2.28e^{-2.3U} - 0.03U + 0.52 \tag{14}$$

where

- $\overrightarrow{F}^{ij}_{cr}(t)$ is the force applied to robot $i$ by robot $j$ at time $t$. $\overrightarrow{Fx}^{ij}_{cr}(t)$ and $\overrightarrow{Fy}^{ij}_{cr}(t)$ are respectively the $x$ and $y$ components of $\overrightarrow{F}^{ij}_{cr}(t)$.
- $\|p_{ij}(t)\|$ is the distance between robots $i$ and $j$. The term $\left[\frac{1}{\|p_{ij}(t)\|^2}\right]$ correlates the force between each pair of robots to their inverse square distance. Therefore, the robots in close vicinity apply large magnitude forces to each other while they do not apply significant forces to the robots which locate very far.
- $X_{ij} = x_i - x_j$ and $Y_{ij} = y_i - y_j$ where $(x_i, y_i)$ is the relative position of robot $i$ and $(x_j, y_j)$ denotes the relative position of robot $j$. It is obvious that $\|\overrightarrow{Y}_{ij}\|$ denotes the magnitude and $\left[\frac{\overrightarrow{Y}_{ij}}{\|\overrightarrow{Y}_{ij}\|}\right]$ is the direction of the vector $\overrightarrow{Y}_{ij}$ (either +1 or −1).
- $\mu_1$, $\mu_2$ and $\mu_3$ are constant coefficients for tuning acceleration of the robots. $\mu_1$ is the Y-component repulsing coefficient and $\mu_2$ is the Y-component attracting coefficient while $\mu_3$ is the X-component attracting coefficient.
- $D_1$ is a design parameter that specifies the desired distance interval between the neighboring robots. We defined $D_1$ using the Eq. (9) to be equal to the optimization results.
- $D_2$ defines the margin of the area that a robot applies forces to the other robots. Logically for line formation $D_2$ should be bigger than $D_1$ and smaller than $2D_1$. Moreover, it is necessary that each robot be always located inside the detection range of at least another robot in order to perform swarm formation behaviors, thus $D_1$ and $D_2$ should always be smaller than $\Delta_d$, $(0 < D_1 < D_2 < \Delta_d)$.

The design of the above equations is inspired by the Hooke's law, thus the forces are similar to the forces in the physical springs. Hence, the robots try to minimize their X-component distance to zero and to maintain a distance of $D_1$ (that is the optimized distance) in their Y-component distance (see Fig. 10). Since the X-axis in the robots is selected to be toward the air-flow direction $\overrightarrow{U}$, the robots will line up cross-wind with constant distance of $D_1$ towards the Y-Axis.

Using the above equation, the total "cross-wind line-up" force $\overrightarrow{F}^{i}_{cr}(t)$ for robot $i$ is determined as:

$$\overrightarrow{F}^{i}_{cr}(t) = \sum_{j=1; j\neq i}^{N} \overrightarrow{F}^{ij}_{cr}(t) \tag{15}$$

It is worth to mention that, although the summation of the force is over all the other robots (N), only those within the detection range $(\Delta_d)$ of robot $i$ which are closer than $D_2$ actually effect the value of $\overrightarrow{F}^{i}_{cr}(t)$.

### 3.2 Robot-to-environment forces

The low level of autonomous navigation of a robot relies on the ability of the robot to simultaneously achieve its target goal and avoid the obstacles in the environment. To avoid the obstacles, a reactive potential field control method (Khatib 1986) is used. Figure 10b is an example that shows the virtual potential forces applied to a robot in an environment. Considering $M$ range sensors, we define the forces applied to robot $i$ by its surrounding environment as:

$$\overrightarrow{F}^{i}_{obs}(t) = \sum_{j=1}^{M} \frac{c_1}{|d_i(j)|^n} \overrightarrow{(Vec_i j)} \tag{16}$$

Since $d_i(j)$ is simply the distance between robot $i$ and an obstacle that is reported by the range sensor $j$, the force is an inverse function of the distance of the robot to the surrounding obstacles. $\overrightarrow{Vec_i j}$ is a predefined vector whose magnitude is

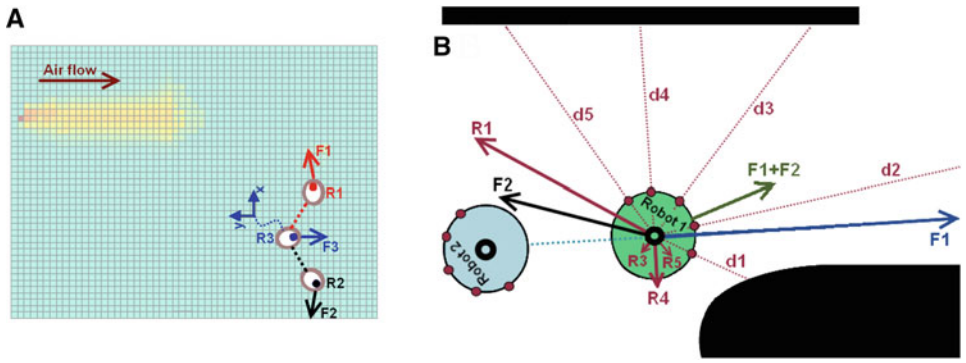


**Fig. 10** **a** Cross-wind line-up behavior; forces applied to the robots based on Eqs. (10–17). *F1* demonstrate the total forces applied to *R1* from *R2* and *R3*. *F2* and *F3* present the total forces applied to *R2* and *R3* respectively. **b** Obstacle avoidance for a robot with five range sensors. **d1–d5** The distance measured by the sensors. *R1–R5* The artificial repulsive forces. "*F1*" represents the artificial robot-to-robot force and "*F2*" illustrates the summation forces of obstacle avoidance. Vector "*F1+F2*" shows the total force applied to robot 1

set to one and its direction is from sensor $j$ toward the center of robot $i$. $c_1$ is a positive coefficient and $n$ is an even integer parameter.

### 3.3 Swarm movements

An unanswered question is that "what should the swarm do if none of the robots detect any odor patches after performing the cross-wind line-up formation?" Implementing the virtual force in Eqs. (15) and (16) will converge to a steady-state line topology for the robots. If none of the robots detect any odor clue for a long time, it means that with high probability there is no odor source in the coverage area of the swarm. In this case the swarm robots should move spatially and explore the environment. Several different search and exploration strategies namely zig-zag casting, spiral movements, random or BRWs, levy taxis, etc, can be taken. As stated in the introduction, this challenge is not in the scope of this paper; however, in any of these strategies the best spatial formation for the swarm is still the found cross-wind line-up configuration that the distance between the robots is proportional to the wind speed.

As an example of swarm movements, one tactic is that if the swarm robots hold the desired formation and still do not detect any odor plume, they move up-wind while keeping their line formation. Hence, they will sweep and cover the environment toward up-wind. We do not claim that this movement strategy is a perfect strategy (and it is not the goal of this paper to show that), but this is only a sample strategy that we use to show how the formation configuration can be hold while the swarm moves. For the swarm to have a desired movement trajectory, each robot should move in the space in the correct direction. To implement this movement strategy, we define $\overrightarrow{F}^{\,i}_{G}(t)$ that is a virtual force applied to robot $i$ at time $t$ towards the swarm's goal. $\overrightarrow{F}^{\,i}_{G}(t)$, in this example, is equal to an up-wind control virtual force, $\overrightarrow{F}^{\,i}_{G}(t) = \overrightarrow{F}^{\,i}_{UpW}(t)$ where:

$$\overrightarrow{F}^{\,i}_{UpW}(t) = \begin{cases} 0\,, & |\overrightarrow{F}^{\,i}_{cr}(t)| > F_{th} \\ -\alpha \overrightarrow{U}_{i}(t)\,, & |\overrightarrow{F}^{\,i}_{cr}(t)| \leq F_{th} \end{cases} \tag{17}$$

$F_{th}$ is a threshold value for the forces applied to a robot, $\alpha$ is a constant positive coefficient and $\overrightarrow{U}_{i}(t)$ is the airflow vector that the robot $i$ has measured at time $t$. The above formula checks if $|\overrightarrow{F}^{\,i}_{cr}(t)|$ is bigger than a defined threshold or not. If $|\overrightarrow{F}^{\,i}_{cr}(t)|$ is very small it means that the resultant virtual forces applied to robot $i$ are near zero, i.e, the topology of the robot and its neighbors is in the form of a cross-wind line and it is in its steady state. In this case a force in the opposite direction of the airflow is applied to the robot $(-\alpha \overrightarrow{U}_{i}(t))$ and robot moves toward up-wind direction.

### 3.4 The total force

The total force applied to a robot in "cross-wind line-up" behavior is:

$$\overrightarrow{F}^{\,i}_{s} = \overrightarrow{F}^{\,i}_{cr} + \overrightarrow{F}^{\,i}_{obs} + \overrightarrow{F}^{\,i}_{G} \tag{18}$$

For a swarm of $N$ individual robots in Euclidean plane, denoting $\theta^i(t)$ as the steering angle of robot $i$ at time $t$, the desired direction of motion of robot $i$ is given by:

$$\theta^i_d(t) = \arctan\left(\overrightarrow{F}^{\,i}_{y}(t), \overrightarrow{F}^{\,i}_{x}(t)\right) \tag{19}$$

where $\overrightarrow{F}^{\,i}_{y}(t)$ and $\overrightarrow{F}^{\,i}_{x}(t)$ represent the $x$ and $y$ components of the force $\overrightarrow{F}^{\,i}_{s}$. Now, a proportional controller is used for the orientation dynamics of the robot:

$$w_i(t) = -\lambda\big(mod\big((\theta_i(t) - \theta^i_d(t)) + \pi, 2\pi\big) - \pi\big) \tag{20}$$

where $\lambda$ is a positive proportional gain. Finally, the next velocity of the robot $\overrightarrow{v}_{i}(t)$ is calculated based on its last

velocity $\overrightarrow{v}_i(t-\Delta t)$ and the forces applied to it $\overrightarrow{F}^i(t)$:

$$\overrightarrow{v}_i(t) = \overrightarrow{v}_i(t-\Delta t) + \eta \overrightarrow{F}^i_s(t)\Delta t \tag{21}$$

while $\eta$ is a constant coefficient multiplied to the acceleration of the robot.

The robots maintain cross-wind line-up behavior until one (or some) of them gets into an odor plume by sensing odor concentrations higher than a defined threshold. Plume tracking is not in the scope of this paper, however, a robot which gets into the odor plume can perform another behavior to inform the other robots to get into the plume and track it.

## 4 Validation

The presented method was validated in both simulations and realistic experiments.

### 4.1 Simulations

The method was tested in several different simulation environments containing obstacles with different number of robots. This section goes to the details of these simulations and presents the results.

#### *4.1.1 Testing environment*

Models of several testing environments were given to ANSYS Fluent CFD[1] software to simulate odor sources and provide odor concentration data. The olfactory data generated by ANSYS Fluent was exported to Matlab to be used in simulations. One of the environments designed for these simulations is depicted in Fig. 11. The dimension of designed arenas for simulations was varied from 4×6 m to 30×40 m. The airflow was ventilated from the inlet side (left) with different speeds from 0.5 to 20 m/s. In the environments with obstacles, the flow velocity varies in different parts of the arena. Figure 12 shows several 3D snapshots of an odor plume propagation during the time in one of the tested scenarios. As shown in the simulation snapshots, the odor propagation is time variant and under turbulent flow. Although the odor plume was simulated in 3D, the robots move in the floor with their gas sensors always at the same height, so, only the odor concentration measured in the 2D plane at the height of the sensors is relevant to the robots' decisions. We extracted the odor concentrations and airflow velocities of 10 cm height from the 3-D odor plumes and fed it to the robots in the simulations. Figure 13 presents some snapshots of an extracted 2-D odor plumes in one scenario.

[1] ANSYS Fluent CFD, "FLUENT user's manual" Software Release, vol. 6, 2006.

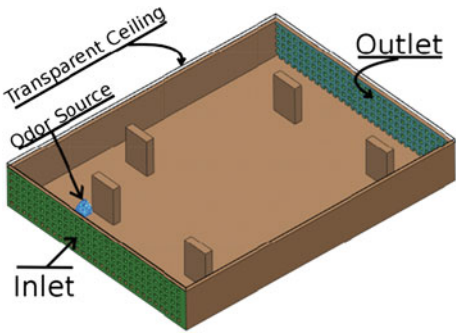


**Fig. 11** The model of a testing environment with 4 × 6 m dimensions

#### *4.1.2 Robots*

Robots were simulated in Matlab as independent entities with no shared variables. The environmental data including odor concentrations, wind speeds and obstacles locations are shared with the robots such that the robots can measure the odor concentration and air-flow speed of their places. Robots are able to measure their distances to the obstacles existing in the neighborhood or to the other neighboring robot. The neighborhood range is an adjustable parameter that can be modified in different tests. The wind-biased potential forces (explained in Sect. 3) were implemented for the movement control of the robots.

Figures 14 and 15 show the virtual forces that the swarm robots generate in the "cross-wind line-up" behavior in different configurations. Each arrow in a place shows the magnitude and the direction of virtual forces that would be applied to another robot if it was located in that place. By adding (or removing) robots to these scenarios the configuration of forces will change, however, these figures only show the virtual forces in the current setup of the figures before adding another robot. These forces are obtained by implementing the Eqs. (10–14). As shown in these figures, the wind direction affects the virtual forces amplitudes. The red "X" marks in each figure show the locations that the virtual forces converge to.

#### *4.1.3 Validation*

Figure 16 shows a series of snapshots during a simulation that show the functionality of the method. The first frame of this figure shows that 10 robots are released randomly in one part of the environment. The next frames demonstrate the cross-wind line-up behavior, where they get apart from each other toward the cross-wind direction. The last frame shows that a robot (the red one) gets into the plume and detects it. Since the wind speed was 5 m/s in this example, the individual robots computed their desired distance ($D_1$) using Eq. (14) as 0.37 m. Figure 16 shows that the robots tend

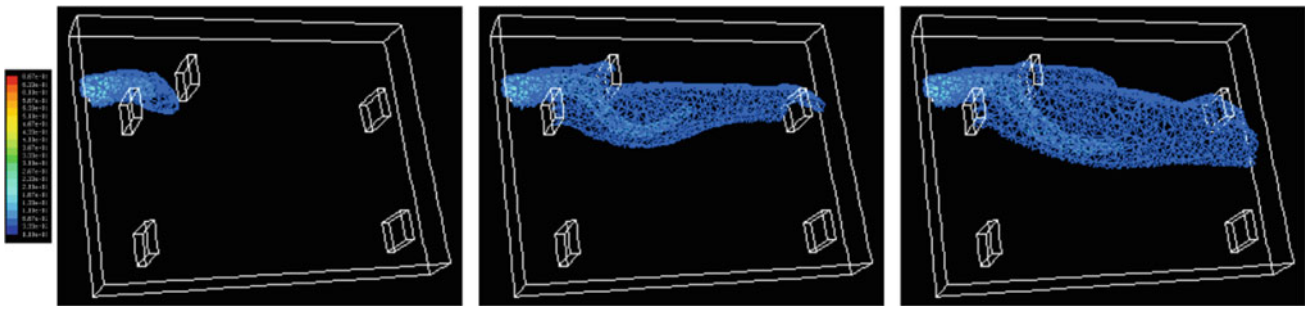

**Fig. 12** ANSYS Fluent three dimension simulations; contours of mass fraction of ethanol propagated in the testing environment of Fig. 11

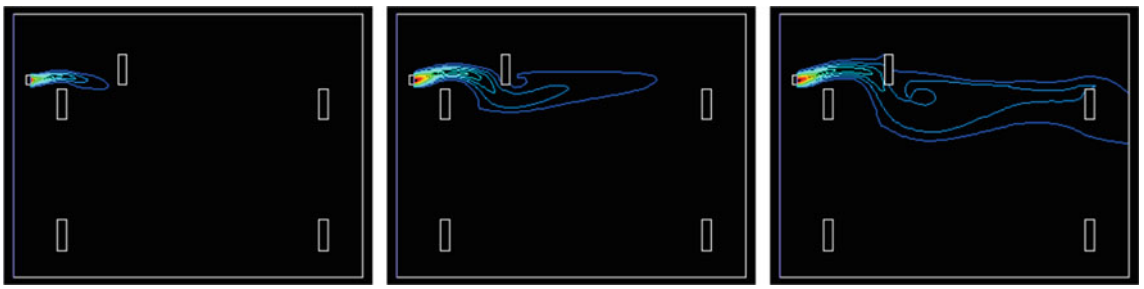

**Fig. 13** Extracted 2-D odor contours of mass fraction of ethanol propagated in the testing environment of Fig. 12 during the time

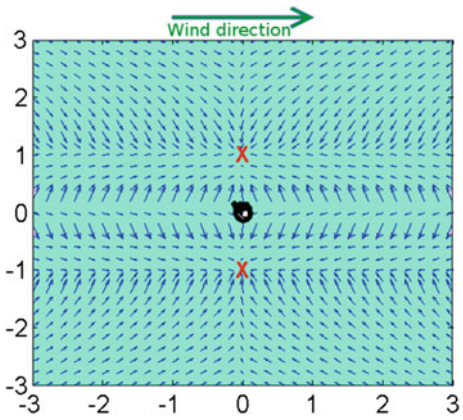


**Fig. 14** Virtual forces generated by a robot when the wind direction is *left* to *right*. The *red X* marks show the locations that the virtual forces converge to. If another robot is added to this system, it will move to one of the marked places (Color figure online)

to reach to the analytic optimal configuration. In this test, the coefficient parameters of the method were set as following: $\Delta_d = 1$ m, i.e. the range of communication between the robots is considered to be 1 m, $\mu_1 = 2$ and $\mu_2 = \mu_3 = 1, \eta = 0.2, \lambda = 0.1, c_1 = 1$, based on the dynamics of simulated robots to achieve a maximum speed of 0.1 m/s.

Since this paper has focused on swarm formation strategies and swarm movement is not in the scope of this paper, we do not evaluate this latter issue here, however, one simulation that shows the functionality of the method with considering the movement for the swarm (described in Sect. 3.3) is shown in Fig. 17. In this test, we intentionally did not put any odor source in the environment to better demonstrate this behavior. The robots expand toward cross-wind in a line and when they are stable they start to move up-wind. The swarm's topology changes with the environmental changes dynamically. The robots cover a large area towards up-wind, searching for any possible odor plume. In the other simulations and experiments, $F^i_{UpW}(t)$ in Eq. 18 is considered zero to disable the up-wind movements of the swarm and only evaluate the formation strategy.

### *4.1.4 Evaluation*

The method was tested in a large environment ($30 \times 40$ m) with 5 and 10 robots repeatedly. Figure 18 shows a part of this environment that is $10 \times 15$ m and includes an ethanol source. The release rate was set to 0.01 g/s and the wind speed was 0.5 m/s. To evaluate the optimization results we measured the plume detection ability of swarm robots in two different formation strategies; 2-D hyperball formation (similar to (Gazi and Passino 2004)) and cross-wind line formation strategy and we manually set the parameter of distance between the robots ($D_1$) to 0.5, 1 and 2 m in different tests to find the best configuration. Each test was repeated for 20 times for every formation and value of $D_1$. If at least one robot could detect the odor plume in less than one minute after the swarm formation was established, we consider a success in plume detection. The number of successfully detecting the odor plume was counted.

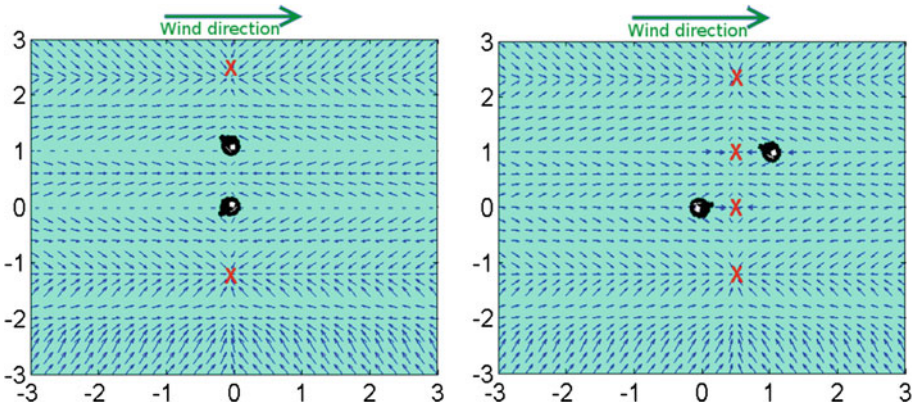


**Fig. 15** Virtual forces generated by two robots. *Left* the robots are already on a cross-wind line. *Right* the robots are not on a cross-wind line, thus, their configuration is not stable

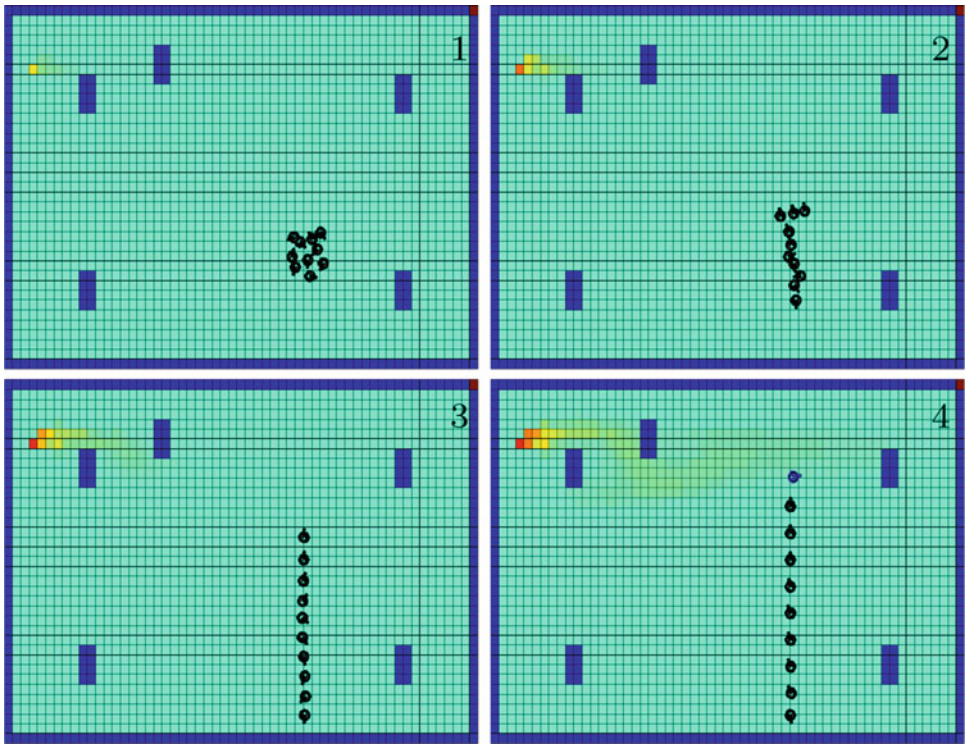


**Fig. 16** 10 swarm robots performing cross-wind line formation (Color figure online)

The results, in Fig. 19, show that the best performance between tested configurations is the one with cross-wind line up formation when $D_1$ is 1 m. On the other hand, using the results of sensor placement optimization in Sect. 2 [Fig. 7a and Eq. (9)], in the conditions of these simulations, the best formation strategy is line formation with $D_1 = 1.22$ m. The best configuration between the simulated ones is very close to the found analytic formation. This validates the optimization achievements.

## 4.2 Experimental results

In addition to simulations, the method was experimented with our currently available robotic facilities.

### *4.2.1 The robots*

A set of iRobot Roomba[2] robots were upgraded with small laptop computers (ASUS EeePC901) running ROS[3] to control the robots. The robots were equipped with Laser range finders (Hokuyo URG-04LX) for obstacles avoidance. Adaptive Monte Carlo localization (AMCL[4]) libraries were used in ROS to localize the robots in the environments. WifiComm[5] was used in ROS that allows multiple robots to communicate with each other peer to peer through an ad-hoc network.

[2] http://www.irobot.com.

[3] http://www.ros.org.

[4] http://www.ros.org/wiki/amcl.

[5] http://www.ros.org/wiki/wifi_comm.

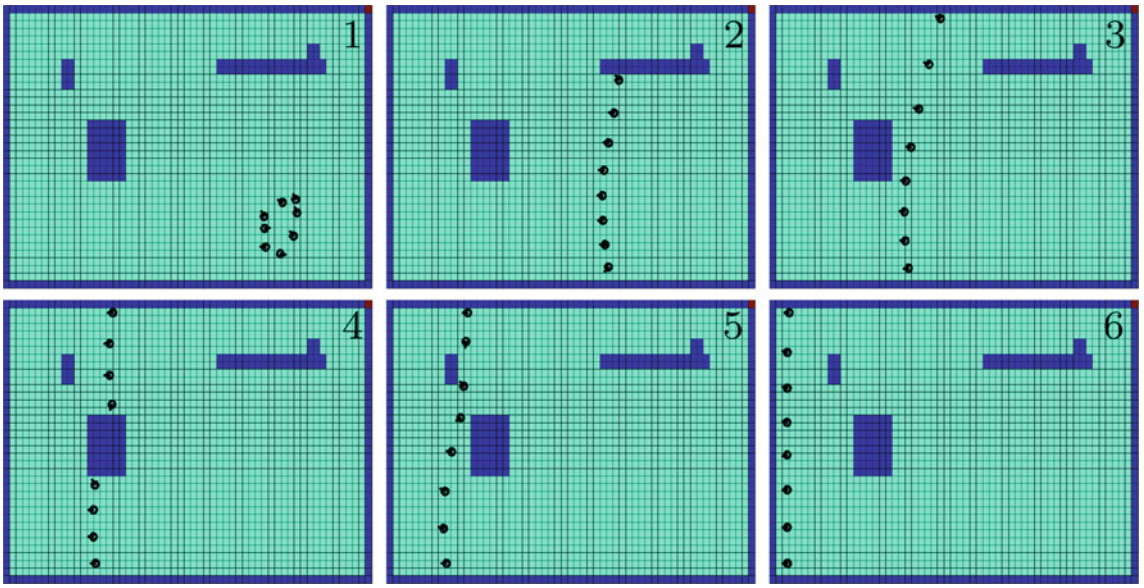


**Fig. 17** Eight swarm robots searching in an environment for possible odor sources. The swarm dynamically changes its topology to deal with environmental changes. There is no odor source in the environment. The airflow is 10 m/s from *left* to *right*, $F_{th} = 0.01$ and $\alpha = 0.1$

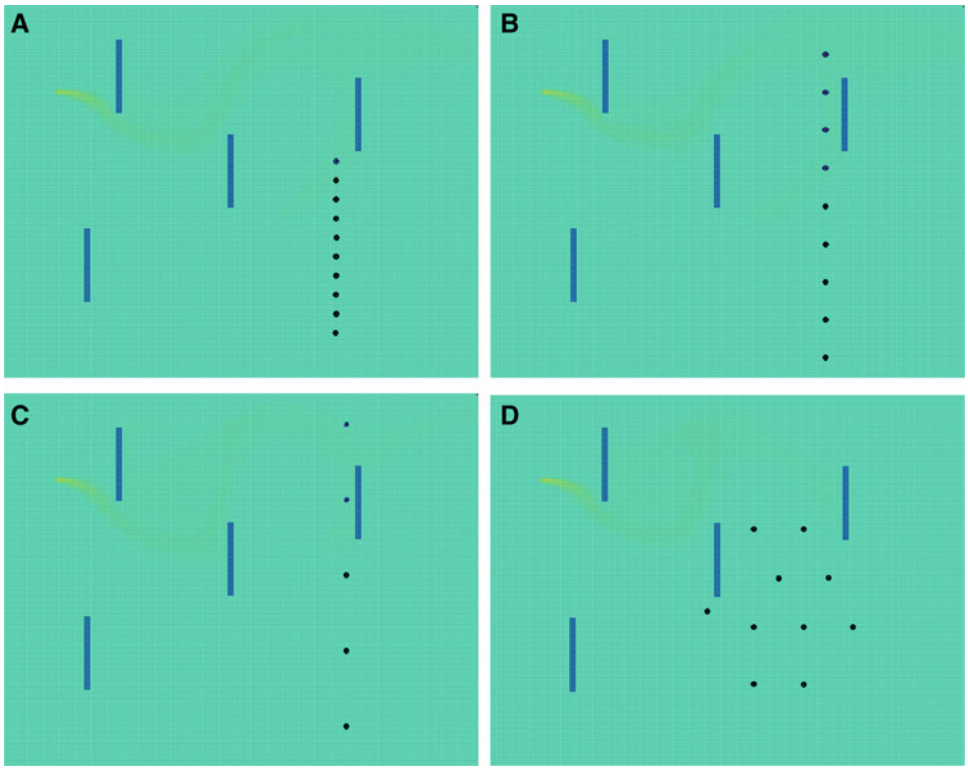


**Fig. 18** A part of a $30 \times 40$ m environment. **a** Line formation, $D_1 = 0.5$ m. **b** Line formation, $D_1 = 1$ m. **c** Line formation, $D_1 = 2$ m. **d** Hyperball formation, distance =1 m. The odor plume is shown in *yellow* (Color figure online)

Each robot was equipped with an e2v MiCS-5521[6] and a Figaro[7] TGS2620 gas sensor to measure the odor concentration. The robots repeatedly broadcasted their localization data, and accordingly, they measured their x-axis and y-axis distances. In these tests, the airflow was intentionally ventilated and controlled towards the x-axis of the robots and wind speed was manually provided (broadcasted) to the robots. Figure 20 presents one of these developed robots.

[6] http://www.e2v.com.

[7] http://www.figarosensor.com.

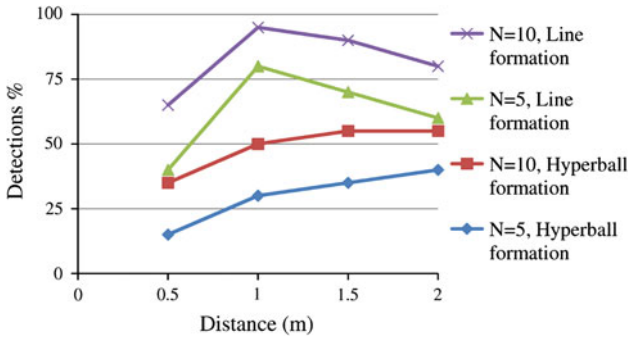


**Fig. 19** Odor plume detection success, during 20 tests in each configuration

**Fig. 20** One of the developed robots containing gas sensors, laser range finder, and iRobot Roomba controlled by a laptop

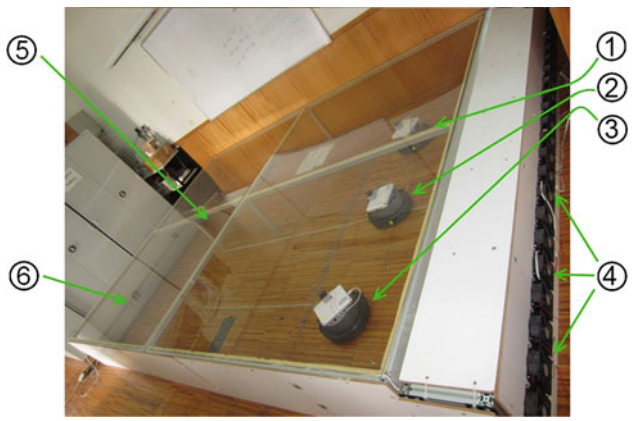


**Fig. 21** The realistic testbed environment. *1*, *2*, *3* Robots, *4* ventilation system, *5* transparent Plexiglas ceiling, *6* odor source

### *4.2.2 Realistic environment*

The method was tested in the reduced scale environment shown in Fig. 21. This arena, with $3 \times 4\,\mathrm{m}^2$ area by 0.5 m height, has controlled ventilation through a manifold that extracts air from the testing environment through a honeycomb mesh integrated into one of the walls. The opposite surface of the environment contains a similar mesh that allows the entrance of clean air that flows through the environment. A controlled ethanol gas source using bubblers is pumped to arbitrary places of the environment through a set of PVC tubes. The ethanol release rate was about 0.01 g/s during the tests. The ceiling of this testbed is covered by a sheet of transparent Plexiglas to be visualized from the outside.

### *4.2.3 Validation*

Figure 21 shows three robots maintaining cross-wind line-up formation finding an odor plume. The robots spatially construct a line formation in the cross wind direction and maintain a specific distance. If one of the robots moves toward a direction, regardless of the cause of this movement, the other robots dynamically move to maintain the line formation.

Similar to the presented simulations, for evaluating the optimization results, the experiments were done with manual values for $D_1$ testing cross-wind line formation and also hyperball (triangle) formation. The wind speed was $0.6 \pm 0.1$ m/s and we set $D_1$ to 0.3, 0.5, 0.7, 0.9, 1.1 and 1.3 m in different tests. Three robots were released randomly 3 m down-wind the source and each test was repeated 15 times and the plume detections were counted. The period of each test was one minute. Figure 22 is an example that shows the output of the e2v sensors in two tests. Each row shows three graphs that correspond to the three robots of the Fig. 21. The first row was taken when the wind speed was $1 \pm 0.1$ m/s and the second row was taken when the wind speed was $0.5 \pm 0.1$ m/s. In both cases the robot 3 (that was close to the center line of the plume) has detected the odor plume whereas robot 1 did not detect the plume. Robot 2, whose distance to robot 3 is 0.7 m in this example, has detected the plume when the wind speed was 0.5 m/s but not when the wind speed was 1 m/s. In each test if at least one of the robots detects the odor plume we consider a success in plume detection.

The results demonstrated in Fig. 23 show that line formation provides more detections and the maximum number of success is reported when the distance between the robots is 0.9 and 1.1 meters. Using Eq. (9), the optimal distance in this configuration is 1.07 m that agrees with the results of the real experiments.

The experiments in the realistic test bed were repeated by changing the wind-speed to $1 \pm 0.1$ m/s. Figure 24 demonstrates the results and shows that when the robots have line formation and their distance is 0.7, the maximum number of detections will be achieved. Based on Eq. (9), the optimal distance in this configuration is 0.71 m that again agrees with the results of these experiments.

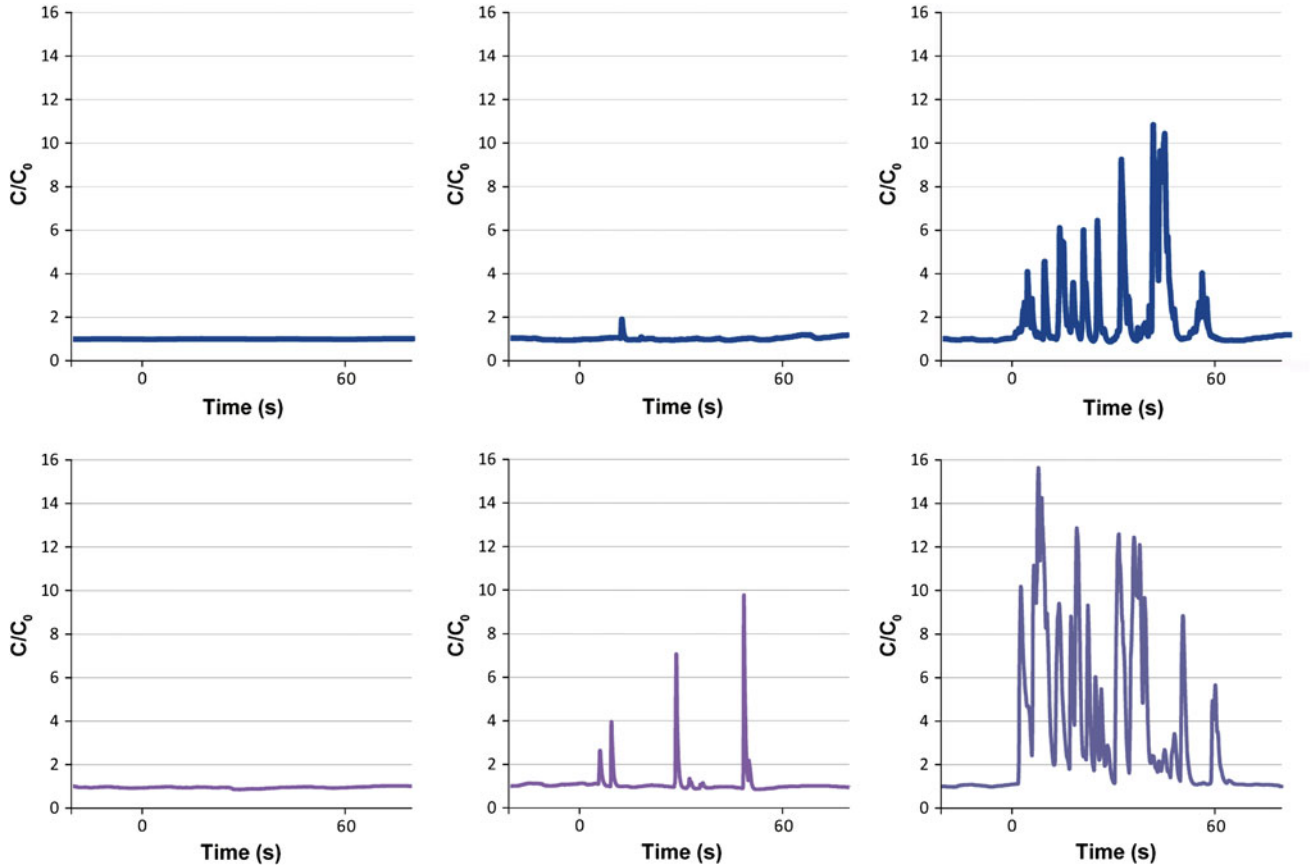


**Fig. 22** The output of e2v sensors of robots 1, 2 and 3 in Fig. 21 from *left* to *right* in each *row* respectively. The wind speed was $1 \pm 0.1$ m/s in the first row and $0.5 \pm 0.1$ m/s in the *second row*

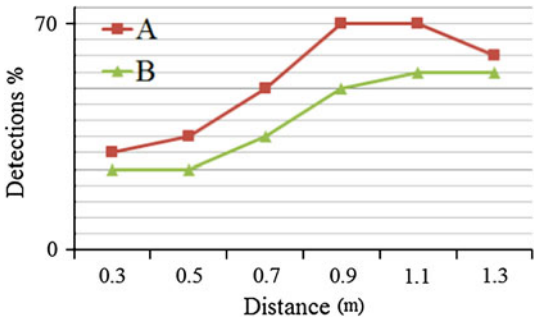


**Fig. 23** Successful detections rate against the distance between the neighboring robots when the wind speed is $0.6 \pm 0.1$ m/s. **a** Line formation, **b** hyperball formation

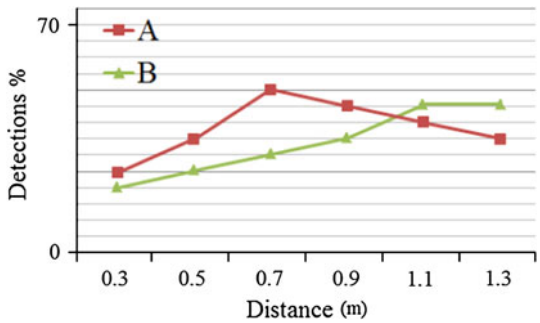


**Fig. 24** Successful detections rate against the distance between the neighboring robots when the wind speed is $1 \pm 0.1$ m/s. **a** Line formation, **b** hyperball formation

## 5 Conclusions

Considering no movement for a network of robotic gas sensors, their optimal spatial formation to maximize the probability of detection of odor plumes was studied. The topology of all of the optimal solutions was line configuration toward cross wind direction, with equal distance between each pair of neighboring sensors. Regardless of number of sensors, the optimal distance between neighboring pairs depends on the wind speed. A mathematical function that can accurately estimate the optimal distances based on the wind speed was computed by nonlinear regression estimation. Moreover, swarm robotics wind-biased attractive/repulsive virtual forces were designed to emerge to the optimal configurations. The method was tested and validated in simulations and in a reduced scale realistic environment. The results verify the

functionality of the swarming formation strategy and also validate the obtained optimization results.

## References


Arshak, K., Moore, E., Lyons, G., Harris, J., & Clifford, S. (2004). A review of gas sensors employed in electronic nose applications. *Sensor Review*, *24*(2), 181–198.

Balkovsky, E., & Shraiman, B. (2002). Olfactory search at high Reynolds number. *Proceedings of National Academy of Science*, *99*(20), 12589–12593.

Briggs, G. (1973). *Diffusion estimation for small emissions ATDL, contribution file No. 97*. Oak Ridge, TN: Air Resources Atmospheric Turbulence and Diffusion Laboratory, NOAA.

Cheng, K., Acevedo-Bolton, V., Jiang, R., Klepeis, N., Ott, W., Fringer, O., & Hildemann, L. (2011). Modeling exposure close toair pollution sources in naturally ventilated residences:Association of turbulent diffusion coefficient with air change rate.*Environmental science & technology*, *45*, 4016–4022.

Crimaldi, J., Wiley, M., & Koseff, J. (2002). The relationship between mean and instantaneous structure in turbulent passive scalar plumes. *Journal of Turbulence*, *3*(14), 1–24.

Cui, X., Hardin, C., Ragade, R., & Elmaghraby, A. (2004). A swarm approach for emission sources localization. In *IEEE International Conferenceon Tools with Artificial Intelligence*, FL, USA.

Dunbabin, M., & Marques, L. (2012). Robotics for environmental monitoring: Significant advancements and applications. *IEEE Robotics and Automation Magazine*, *19*(1), 24–39.

Ferri, G., Caselli, E., Mattoli, V., Mondini, A., Mazzolai, B., & Dario, P. (2009). SPIRAL: A novel biologically-inspired algorithm for gas/odor source localization in an indoor environment with no strong airflow. *Robotics and Autonomous Systems*, *57*(4), 393–402.

Fu, H.-L., Chen, H.-C., & Lin, P. (2012). APS: Distributed air pollution sensing system on wireless sensor and robot networks. *Computer Communications*, *35*(9), 1141–1150.

Gazi, V., & Passino, K. (2004). Stability analysis of social foraging swarms. *IEEE Transactions on Systems, Man, and Cybernetics, Part B*, *34*(1), 539–557.

Gifford, F. (1960). Peak to average concentration ratios according to a fluctuating plume dispersion model. *International Journal of Air Pollution*, *3*, 253.

Grasso, F., Dale, J., Consi, T., Mountain, D., & Atema, J. (1997). Effectiveness of continuous bilateral sampling for robot chemotaxis in a turbulent odor plume: Implications for lobster chemo-orientation. *The Biological Bulletin*, *193*(2), 215–216.

Hayes, A., Martinoli, A., & Goodman, R. (2003). Swarm robotic odor localization: Off-line optimization and validation with real robots. *Robotica*, *21*(04), 427–441.

Hernandez Bennetts, V., Lilienthal, A., Neumann, P., & Trincavelli, M. (2012). Mobile robots for localizing gas emission sources on landfill sites: Is bio-inspiration the way to go? *Frontiers in Neuroengineering*, *4*, 20.

Ishida, H., Tanaka, H., Taniguchi, H., & Moriizumi, T. (2006). Mobile robot navigation using vision and olfaction to search for a gas/odor source. *Autonomous Robots*, *20*(3), 231–238.

Jones, C. (1983). On the structure of instantaneous plumes in the atmosphere. *Journal of Hazardous Materials*, *7*(2), 87–112.

Kazadi, S. (2003). Extension of plume tracking behavior to robotswarms. In *Proceedings of the IIIS/SCI Conference on Systems,Cybernetics, and Informatics*, Orlando, USA.

Khatib, O. (1986). Real time obstacle avoidance for manipulators and mobile robots. *International Journal of Robotics Research*, *5*(1), 90–99.

Kowadlo, G., Rawlinson, D., Russell, R., & Jarvis, R. (2006). Bi-modal search using complementary sensing (olfaction/vision) forodour source localisation. In *Proceedings of IEEE International Conference onRobotics and Automation*, Orlando, USA.

Krishnanand, K., & Ghose, D. (2008). Theoretical foundations for rendezvous of glowworm-inspired agent swarms at multiple locations. *Robotics and Autonomous Systems*, *56*(7), 549–569.

Legg, S., Benavides-Serrano, A., Siirola, J., Watson, J., Davis, S., Bratteteig, A., & Laird, C. (2012). A stochastic programmingapproach for gas detector placement using cfd-based dispersionsimulations. *Computers & Chemical Engineering*, *47*, 194–201.

Li, F., Meng, Q., Bai, S., Li, J., & Popescu, D. (2008). Probability-PSO algorithm for multi-robot based odor source localization in ventilated indoor environments. *Intelligent Robotics and Applications*, *5314*, 1206–1215.

Li, W., Farrell, J., & Cardé, R. (2001). Tracking of fluid-advected odor plumes: Strategies inspired by insect orientation to pheromone. *Adaptive Behavior*, *9*(3–4), 143.

Lilienthal, A., & Duckett, T. (2004). Building gas concentration gridmaps with a mobile robot. *Robotics and Autonomous Systems*, *48*(1), 3–16.

Lochmatter, T., Aydin, E., Navarro, I., & Martinoli, A. (2010). A plume tracking algorithm based on crosswind formations. In *Proceedings of International Symposium on Distributed Autonomous Robotics Systems*.Lausanne, Switzerland.

Lochmatter, T. & Martinoli, A. (2009). Tracking odor plumes in alaminar wind field with bio-inspired algorithms. In *Experimental robotics*. Berlin, Heidelberg: Springer.

Loutfi, A., Coradeschi, S., Lilienthal, A., & Gonzalez, J. (2008). Gas distribution mapping of multiple odour sources using a mobile robot. *Robotica*, *27*(02), 311–319.

Lytridis, C., Kadar, E., & Virk, G. (2006). A systematic approach to the problem of odour source localisation. *Autonomous Robots*, *20*(3), 261–276.

Marjovi, A., & Marques, L. (2011). Multi-robot olfactory search in structured environments. *Robotics and Autonomous Systems*, *52*(11), 867–881.

Marjovi, A., & Marques, L. (2012). Multi-robot topological exploration using olfactory cues. *Springer Tracts in Advanced Robotics Distributed Autonomous Robotic Systems*, *83*, 47–60.

Marjovi, A., Nunes, J., Marques, L., & de Almeida, A. (2010a). Multi-robot fire searching in unknown environment. *Springer Tracts in Advanced Robotics Field and Service Robotics*, *62*, 341–351.

Marjovi, A., Nunes, J., Sousa, P., Faria, R., & Marques, L.(2010b). An olfactory-based robot swarm navigation method. In *Proceedings of IEEE International Conference on Robotics and Automation*, Alaska, USA.

Marjovi, A., Nunes, J.G., Marques, L., & de Almeida, A.T.(2009). Multi-robot exploration and fire searching.In *IEEE/RSJ International Conference on Intelligent Robots and Systems*, St. Louis, MO, USA.

Marques, L., & de Almeida, A. (2006). ThermalSkin: A distributed sensor for anemotaxis robot navigation. In *Proceedings of 5th IEEE International Conference on Sensors*, South Korea.

Marques, L., Nunes, U., & Almeida, A. (2002). Olfaction-based mobile robot navigation. *Thin Solid Films*, *418*(1), 51–58.

Marques, L., Nunes, U., & de Almeida, A. (2006). Particle swarm-based olfactory guided search. *Autonomous Robots*, *20*(3), 277–287.

Martinez, D., Rochel, O., & Hugues, E. (2006). A biomimetic robot for tracking specific odors in turbulent plumes. *Autonomous Robots*, *20*(3), 185–195.

Meng, Q., Yang, W., Wang, Y., & Zeng, M. (2011). Collective odor source estimation and search in time-variant airflow environments using mobile robots. *Sensors*, *11*(11), 10415–10443.

Miyata, E., & Mori, S. (2011). Optimization of gas detector locations by application of atmospheric dispersion modeling tools. *Sumitomo Kagaku*, *I*, 1–10.

Pasternak, Z., Bartumeus, F., & Grasso, F. (2009). Lévy-taxis: A novel search strategy for finding odor plumes in turbulent flow-dominated environments. *Journal of Physics A: Mathematical and Theoretical*, *42*, 434010.

Press, W., Flannery, B., Teukolsky, S., & Vetterling, W. (2002). Direction set (Powell's) methods in multidimensions. *Numerical Recipes in C++: The Art of Scientific, Computing*, *1992*, 417–424.

Pyk, P., Bermúdez i Badia, S., Bernardet, U., Knüsel, P., Carlsson, M., Gu, J., et al. (2006). An artificial moth: Chemical source localization using a robot based neuronal model of moth optomotor anemotactic search. *Autonomous Robots*, *20*(3), 197–213.

Roberts, P., & Webster, D. (2002). *Turbulent diffusion*. Reston, VA: ASCE Press.

Russell, R., Bab-Hadiashar, A., Shepherd, R., & Wallace, G. (2003). A comparison of reactive robot chemotaxis algorithms. *Robotics and Autonomous Systems*, *45*(2), 83–97.

Russell, R., Thiel, D., Deveza, R., & Mackay-Sim, A. (1995). A robotic system to locate hazardous chemical leaks. In *Proceedings of IEEE International Conference on Robotics and Automation*, Nagoya, Japan.

Sutton, O. (1947). The problem of diffusion in the lower atmosphere. *Quarterly Journal of the Royal Meteorological Society*, *73*(317–318), 257–281.

Vergassola, M., Villermaux, E., & Shraiman, B. (2007). 'Infotaxis' as a strategy for searching without gradients. *Nature*, *445*(7126), 406–409.

Wang, H., Zhang, M., Wang, J., & Huang, M. (2010). Engineering an emergency search and rescue application with wireless sensor network and mobile robot. *International Conference on Measuring Technology and Mechatronics Automation*, *2*, 112–115.

Zarzhitsky, D., Spears, D., & Spears, W. (2005). Swarms forchemical plume tracing. In *Proceedings of the IEEE SwarmIntelligence Symposium*, CA, USA.

## Author Biographies

**Ali Marjovi** has a Ph.D. degree in Electrical and Computer Engineering from University of Coimbra, Portugal in the field of Distributed Olfactory Robotics. He received his M.Sc. degree in Computer Hardware Engineering from Sharif University of Technology, Tehran, Iran, in 2005 and his B.Eng. degree in the same field from the University of Isfahan, Iran in 2003. He is currently a post-doc researcher at the Distributed Intelligent Systems and Algorithms Laboratory, EPFL, Switzerland. His research interests include multi-robot search and exploration, and swarm robotic olfaction.

**Lino Marques** has a Ph.D. deg ree in Electrical Engineering from the University of Coimbra, Portugal. He is currently a Senior Lecturer at the Department of Electrical and Computer Engineering, University of Coimbra, and he heads the Embedded Systems Laboratory of the Institute for Systems and Robotics from that university (ISR-UC). His main research interests include embedded systems, mechatronics, and robotics for risky environment.